

A Density Functional Theory Calculations-Based Approach that Predicts Layered Materials with Emergent Structures

Sven P. Rudin*

Los Alamos National Laboratory, Los Alamos, New Mexico 87545, USA

E-mail: srudin@lanl.gov

Abstract

Recent work shows that density functional theory calculations accurately describe materials exhibiting turbostratic disorder between layers of incommensurate constituents. These calculations approximate one of the constituents as a finite island between continuous layers of the other constituent. This island approximation allows equal treatment of all relative angles between the interleaved layers, and it removes the requirement of a unit cell that is commensurate with both layers. The work presented here uses this approximation to search for new layered materials that exhibit turbostratic disorder and magnetic structure. In a first application, the approach finds the recently synthesized $\text{SnSe}_2\text{-VSe}_2$ system. The approach predicts a stable $\text{Fe}_3\text{Ge-VSe}_2$ structure and multiple stable structures that interleave Mn_xSe_y layers with VSe_2 layers. These Mn_xSe_y layers exhibit emergent structures and stability.

The theoretical approach outlined here proposes to accelerate the experimental discovery of new layered materials. Recent efforts in creating new materials that layer known 2D materials reveal properties and phenomena of both scientific and practical interest.¹ Designing materials with a

*To whom correspondence should be addressed

desired functionality becomes possible by choosing the individual constituents with specific properties, provided the interleaved constituents form a kinetically stable material. Recent advances in high-throughput calculations of, e.g., thermoelectric properties² enable a highly informed choice of possible constituents; recent advances in synthesis methods enable their assembly into nanostructured materials with high thermoelectric efficiency.³⁻⁵ Desired properties can also be strongly influenced by the interfaces between the layers, in particular low thermal conductivity benefits from interleaving layers with lattices that remain incommensurate.⁶ Allowing for incommensurate layers significantly widens the pool of possible combinations in the search for new materials.

Confinement at the nanoscale also allows the constituents to stabilize in structures that are neither stable as an isolated 2D form nor a slice of a stable bulk crystal structure. Such emergent structures can be discovered serendipitously, guided by intuition and chemical similarity. Theoretical guidance can focus experimental efforts on systems more likely to show success. Density functional theory (DFT)⁷ calculations can provide such guidance, testing all possible structures constructed from systematically chosen combinations of chemical elements. This type of approach is successfully applied to, e.g., calculating the defect energies and site preference of all possible dopants in lithium battery materials.⁸ In the search for new layered materials, however, the large number of possible structures and chemical element combinations makes this kind of search costly. In addition, for each probed system unit cells must be constructed that are commensurate with each pair of potential structures of the layered constituents – a challenging task when neither the layers' lattice constants nor their relative orientation are known beforehand.

The approach outlined here proposes to accelerate such theoretical searches by using unit cells that approximate one constituent as a finite island between continuous layers of the other constituent. This truncation, used in Ref. 9, removes the requirement for an *a priori* constructed unit cell that is commensurate with both layers. The finite island possesses significantly more freedom to rearrange its ions during DFT optimization, so multiple final structures become accessible from a single starting configuration. The search is further accelerated because each probed unit cell can be much smaller than would be required for a complete, commensurate unit cell. Edge effects

arise, but experience shows that, after optimization, the core ions in the islands either distinctly resemble sections of a crystal structure or they appear randomly dispersed (see Fig. 1). The former, promising systems can serve to guide synthesis efforts. Details of these promising structures can also serve to construct unit cells in which both constituents are continuous layers, unit cells with which further theoretical study can test for interesting properties. Experience with such unit cells shows their optimization takes on the order of five times longer than the typical optimization of an unit cell with one layer approximated as a finite island. This difference translates into an acceleration of the theoretical search for new materials that is at least five-fold, which represents a lower limit because it includes only the effect of using smaller unit cells and not the other points raised above.

The approximation with a finite island arises in applying DFT to understand a material exhibiting turbostratic disorder, $[(\text{SnSe})_{1+y}]_m(\text{VSe}_2)_n$.⁹ Layered materials with turbostratic disorder consist of parallel-layered constituents where the translation parallel to the layer and rotation normal to the layer are random on average.^{10,11} Such disorder leads to ultralow thermal conductivity across the layers.⁴ Layered materials with turbostratic disorder can also be designed for a tunable superconducting transition temperature.¹² In $[(\text{SnSe})_{1+y}]_m(\text{VSe}_2)_n$, n triatomic thick (001) slices of VSe_2 alternate with m diatomic thick (001) slices of SnSe . The two constituents exhibit a mismatch in formula units per area, the misfit parameter $1 + y$. Approximating SnSe as a finite island between continuous layers of VSe_2 allows DFT calculations that treat equally all angles between the constituents.

Given the approximation's accurate description of an existing system, this work uses it to predict systems that could potentially be synthesized. The investigated systems retain VSe_2 as one constituent and construct the other from two period four elements to probe the latter's viability when interleaved with VSe_2 . Specifically, three combinations are investigated: (1) Sn_xSe_y , to test whether the approach delivers the recently discovered SnSe_2 - VSe_2 structure,¹³ (2) Fe_xGe_y and (3) Mn_xSe_y . The inclusion of magnetic ions aims to probe for systems that exhibit turbostratic disorder and magnetic structure.

Table 1: Details of predicted composition and structure of layers that form kinetically stable systems layered with VSe_2 . The composition of the layer can differ from that of the (presumed) bulk structure from which it is sliced. The emergent Mn_3Se_2 structure cannot currently be identified as a slice of a known bulk structure. The misfit parameter $1 + y$ equals the ratio of in-plane unit cell area of the predicted structure to that of VSe_2 , evaluated in the optimized island unit cell.

composition		bulk structure type	slice	$1 + y$
bulk	layer			
SnSe	SnSe	rock salt	[001]	1.19
SnSe ₂	SnSe ₂	cadmium iodide	[001]	1.36
Fe ₃ Ge	Fe ₂ Ge	auricupride	[001]	1.39
Mn ₂ Se	MnSe	iron stannide	[001]	1.52
	Mn ₃ Se ₂			1.40
Mn ₃ Se	Mn ₂ Se	auricupride	[001]	1.38
MnSe ₂	MnSe ₂	cadmium iodide	[001]	1.24
MnSe ₂	MnSe ₂	molybdenum disilicide	[100]	2.6

Table 1 summarizes the systems predicted to form kinetically stable layers between VSe_2 layers. For each system, the table lists the composition found in the layer. Most layers approximate a slice from a presumed bulk structure with a sometimes different composition. The structure type of the presumed bulk structure is given, along with the orientation of the slice. The last column lists the misfit parameters, calculated from the ratio of the two constituents' approximate lattice parameters.

DFT calculations using the VASP package^{14,15} serve to optimize initial structures and explore systems that show promise. The calculations allow spin polarization and evaluate the energies and forces in the generalized gradient approximation of Perdew, Burke, and Ernzerhof.¹⁶ The electronic structure is treated with a Fermi-Dirac smearing of width 0.1 eV and converged to 10^{-5} eV. The stopping criterion for ionic relaxation is 10^{-4} eV. The calculations employ a single k-point (Γ). The contributions from the van der Waals interaction are described by the DFT-D2 pair-wise empirical approximation of Grimme with the default values for the parameters.¹⁷ The islands' initial structures are isostructural to truncated slices of binary crystal structure types including auricupride, cadmium iodide, iron stannide, molybdenum disilicide, and rock salt. Typical unit cells contain between 18 and 70 ions in the island structure and either 36 or 49 VSe_2 primitive

cells in the continuous VSe_2 layer. The initial structures are relaxed via the conjugate gradient method with no imposed constraints.

For each of the three chemical combinations, the optimization of the initial structures leads to a few promising cases among many inauspicious cases. The promising cases, detailed below, are characterized by intact VSe_2 layers and islands exhibiting a core region with well-defined structure. The cases that show no promise in general do so very clearly: the island structures often appear disordered, and in some cases the VSe_2 layers disintegrate.

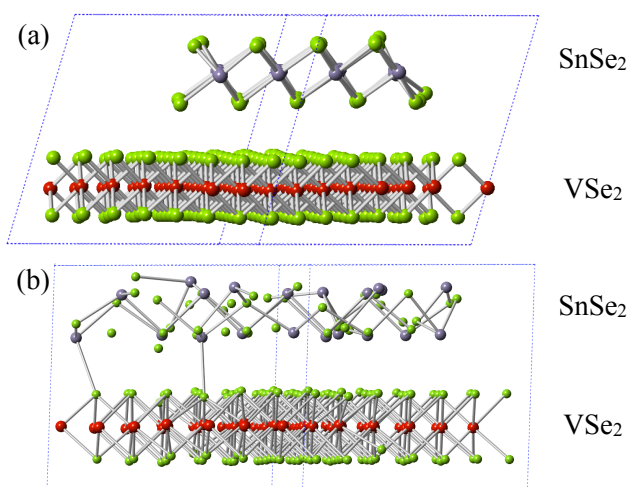


Figure 1: Side views of optimized unit cells containing a complete VSe_2 layer and a $SnSe_2$ island structure. (a) Optimization of a $SnSe_2$ island in the cadmium iodide structure results in a promising case, in agreement with experiment.¹³ (b) Starting from an initial $SnSe_2$ island in the molybdenum disilicide structure results in an agglomeration of ions without much structure. V, Se, and Sn ions are colored red, green, and grey, respectively. Bars represent V-Se and Sn-Se bonds with lengths of up to 3 Å.

Figure 1 shows two optimized unit cells for VSe_2 layers confining a $SnSe_2$ island, exemplifying a promising and an unfavorable case. The promising $SnSe_2$ island (Fig. 1(a)) stabilizes in the 1T structure, approximately a triatomic thick (001) slice of $SnSe_2$ with the same cadmium iodide crystal structure type as VSe_2 . The layers differ in orientation by 26° . The V-V bond lengths exhibit a narrow distribution (with standard deviation $\sigma = 0.02$ Å) centered around 3.28 Å, while the Sn-Sn bond lengths average 3.85 Å with a much wider $\sigma = 0.26$ Å. Optimizing a unit cell with roles reversed (i.e., complete $SnSe_2$ layer and VSe_2 island) leads to a more accurate estimate

of 3.82 Å ($\sigma = 0.02$ Å) for the Sn-Sn bond lengths. These values result in a misfit parameter of 1.36, somewhat larger than the experimental value of 1.25.¹³ Optimization of a SnSe-VSe₂ unit cell with a SnSe island based on the rock salt structure (not shown here) results in similar good agreement (see Ref. 9) with experiment.¹⁸ The poorly structured island in Fig. 1(b) represents one of many unfavorable cases. Among all the optimized unit cells that layer VSe₂ with a Sn-Se island, only two qualify as promising cases, and these two show the same structure as the two synthesized systems with this chemistry.

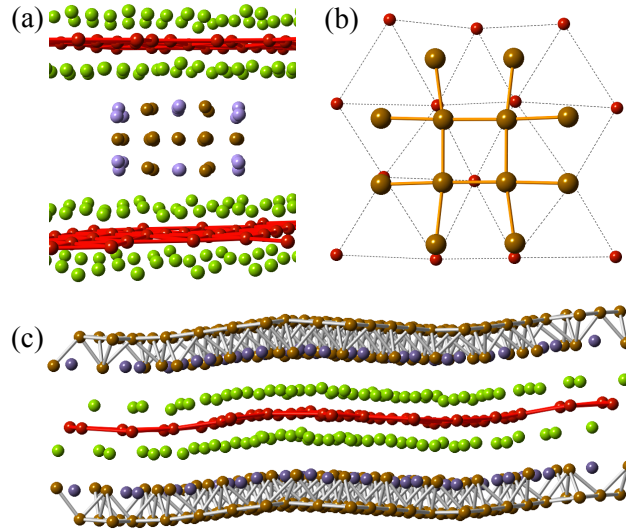


Figure 2: Predicted layered Fe₃Ge-VSe₂ system. Optimized island in (a) side view and (b) top view showing orientation of Fe ions over V ions. (c) Side view of optimized unit cell with complete VSe₂ and Fe₃Ge layers. V, Se, Fe, and Ge ions are colored red, green, brown, and lavender, respectively.

Having successfully reproduced the known structures that interleave VSe₂ with Sn-Se layers, the approach is used to predict systems that have yet to be synthesized. Figure 2 shows the predicted Fe₃Ge-VSe₂ system. The Fe₃Ge constituent is a triatomic thick (001) slice of bulk cubic ϵ_1 -Fe₃Ge (AuCu₃ structure), exhibiting bond lengths close to that of the bulk material. The Fe₃Ge island has average Fe-Fe bond lengths of 2.48 Å ($\sigma = 0.08$ Å) and average V-V bond lengths of 3.34 Å ($\sigma = 0.19$ Å). An optimized unit cell with complete Fe₃Ge layers and VSe₂ islands has average Fe-Fe bond lengths of 2.55 Å ($\sigma = 0.08$ Å), closer to the measured Fe-Fe bond length of 2.59 Å in bulk ϵ_1 -Fe₃Ge.¹⁹

Optimized island-containing unit cells of the promising cases generally have parallel, planar layers. Approximate unit cells with both layers completed often show a wave-like structure as in Fig. 2(c). The spatial oscillations are commensurate with the unit cell and arise from strain imposed on one or both layers. For example, the unit cell in Fig. 2(c) contains a VSe_2 layer with in-plane lattice vectors that are around 3% larger than those of bulk VSe_2 , while the in-plane lattice vectors of the Fe_3Ge layer are around 5% shorter than those of bulk Fe_3Ge . With both layers strained, both show the spatial oscillation.

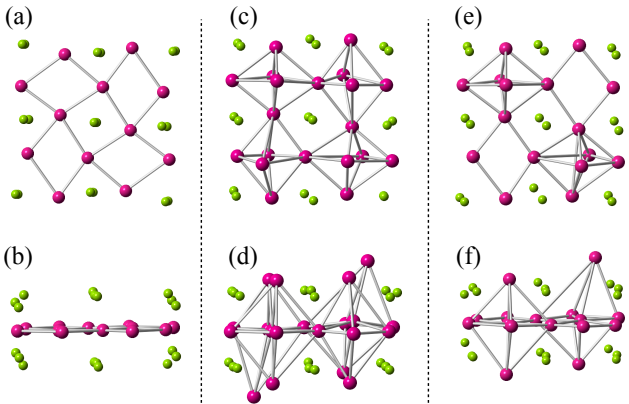


Figure 3: Top and side views of optimized islands (VSe_2 layers not shown) for (a, b) MnSe-VSe_2 , (c, d) $\text{Mn}_2\text{Se-VSe}_2$, and (e, f) $\text{Mn}_3\text{Se}_2\text{-VSe}_2$. Se and Mn ions are colored green and magenta, respectively.

The character of the spatial oscillation of the unit cell in Fig. 2(c) re-emerges in the magnetic structure. Bader analysis of the up and down spin charge distributions serves to assign their sum and difference to charge and magnetic moment, respectively, of the individual ions.²⁰ The magnetic moments on the V ions lie between 0 and $1.6 \mu_B$ and exhibit a spin density wave commensurate with the wave-like structure shown in Fig. 2(c). The same pattern appears in the magnetic moments of the Fe ions, which range between 1.5 and $2.2 \mu_B$. The Bader analysis for the charge distribution suggests a small charge transfer from the Fe_3Ge layer to the VSe_2 layer of approximately 0.2 electrons per Fe ion.

The search for systems interleaving VSe_2 and Mn_xSe_y layers uncovers multiple stable islands, two with closely related structures. Figures 3(a) and (b) show the first island, a finite cut from a triatomic thick (001) slice of MnSe in a form isostructural with iron stannide. The lattice parameter

values average to 3.76 Å. In an optimized unit cell with both MnSe and VSe₂ layers completed, the MnSe layer contains octahedra with Se ions at the apexes and Mn ions forming the central-layer square. These octahedra exhibit a checkerboard rotational pattern with the octahedra rotated by approximately $\pm 7^\circ$.

Figures 3(c) and (d) show the second island containing Mn and Se ions. The Mn₂Se layer resembles a triatomic thick (001) slice of Mn₃Se in a distorted AuCu₃ structure. The lattice parameter values average to 3.58 Å. This structure resembles the previous MnSe island, but with additional Mn ions centered above the Mn diamond shapes of the central monolayer. This reduces the rotation of the MnSe octahedra by approximately 2° . The additional Mn ions sit slightly out of the monolayer formed by the Se ions and do so with unequal amounts, accompanied by a slight in-plane displacement away from high-symmetry positions.

The two independently optimized MnSe and Mn₂Se islands differ essentially only in the eight Mn ions, suggesting possible intermediate systems with less than all eight sites occupied. The optimization of such systems, constructed by selectively removing different numbers of the eight Mn ions, results in stable islands. Comparison of the energies reveals that the most stable system is Mn₃Se₂-VSe₂, which contains four of the eight Mn ions in the pattern shown in Fig. 3(e) and (f). The lattice parameter averages 3.61 Å (i.e., between the averages of the MnSe and Mn₃Se islands). The formation energies of the islands with between zero and eight Mn ions differ at a scale an order of magnitude smaller than room temperature, suggesting a system with potentially interesting properties related to variable composition, rotation of the SeMn octahedra, disorder among occupied Mn sites, and magnetic structure.

In addition to the stable islands shown in Fig. 3, two other Mn_xSe_y systems optimize into stable island structures interleaved with VSe₂. The first is isostructural with SnSe₂-VSe₂. The MnSe₂ layer optimizes with slightly smaller lattice constant 3.65 Å, giving this system a slightly smaller misfit parameter of 1.24. The second system stabilizes with a two monolayer MnSe₂ structure that resembles a section of the molybdenum disilicide structure type. The layer is a [100] slice of the crystal structure with in plane lattice parameters of approximately 3.1 Å and 7.6 Å. The unit

cell outlined by these lattice parameters contain two MnSe_2 formula units, thereby doubling this system's misfit parameter compared to the other systems' typical values.

Calculated formation energies E_f for the five $\text{Mn}_x\text{Se}_y\text{-VSe}_2$ systems provide an estimate for their stability. The values for E_f are calculated for approximate unit cells with completed layers, with the energies for VSe_2 , Mn, and Se in their equilibrium bulk form serving as references. The E_f are at best approximate, as these calculations use a k-point mesh with density $20/\text{\AA}^{-1}$ (computational resources prevent using a finer grid). MnSe_2 in the cadmium iodide structure and MnSe in the iron stannide structure appear most stable with a predicted E_f of approximately -0.1 eV/ion. The Mn_3Se_2 structure has an estimated formation energy of roughly -0.05 eV/ion, and hence lies above the convex hull. MnSe_2 in the auricupride structure requires roughly +0.02 eV/ion to form. No unit cell is constructed for the MnSe_2 system in the molybdenum disilicide structure; the formation energy for this system in the island approximation is approximately +0.07 eV/ion.

The predicted $\text{Mn}_x\text{Se}_y\text{-VSe}_2$ systems exhibit either slices of known Mn_xSe_y bulk crystal structures or form unrelated structures that emerge in the nanoscale confinement. Either option could be expected, as none of the known bulk Mn_xSe_y crystal structures exhibit a 2D character.²¹ Among the known bulk crystal structures with MnSe composition, the high-pressure nickeline structure²² and the rock salt structure²³ can both be sliced into a three monolayer piece that approximates a slice of the cadmium iodide structure type. The known bulk MnSe_2 crystal structure,²⁴ of pyrite structure type, resembles none of the stable island structures. However, the pyrite structure type shares one structural component with the molybdenum disilicide structure type MnSe_2 layer: the MnSe_2 layer exhibits parallel lines that repeat a Se-Mn-Se pattern; the MnSe_2 crystal structure contains the same Se-Mn-Se patterned lines, but instead of aligning parallel the lines lie at oblique angles.

In conclusion, the theoretical approach outlined here proposes to accelerate the experimental discovery of new layered materials as well as the theoretical search for promising systems. It layers two constituents of nanoscale thickness: one from an existing layered material (here VSe_2), the second from sets of chemical elements (here period four elements) to probe for stable structures.

The probing relies on density functional theory calculations to optimize initial structures, with the second layer approximated as a finite island. This approximation dramatically accelerates the theoretical search for new materials because (a) the unit cells contain significantly fewer ions and (b) a single initial structure serves as starting point for multiple final candidate structures. The approach results in predictions of kinetically stable layered materials as guidance for synthesis efforts. The results outlined here specify systems amenable to synthesis: VSe₂ interleaved with either Fe₃Ge or Mn_xSe_y. In particular, Mn_xSe_y-VSe₂ promises interesting behavior including emergent structures, and preliminary synthesis attempts of Mn_xSe_y layered with VSe₂ show promise.¹³

This research is supported by the Department of Energy under Contract No. DE-AC52-06NA25396 and Grant No. LDRD-DR 20140025. The author thanks E. Chisolm, D. Hamann, R. Hennig, O. Hite, D. Johnson, A. Niklasson, B. Revard, and F. Ronning for helpful and encouraging discussions.

References

- (1) Geim, A. K.; Grigorieva, I. V. *Nature* **2013**, *499*, 419–425.
- (2) Chen, W.; Pohls, J.-H.; Hautier, G.; Broberg, D.; Bajaj, S.; Aydemir, U.; Gibbs, Z. M.; Zhu, H.; Asta, M.; Snyder, G. J.; Meredig, B.; White, M. A.; Persson, K.; Jain, A. *J. Mater. Chem. C* **2016**, *4*, 4414–4426.
- (3) Moss, S.; Noh, M.; Jeong, K. H.; Kim, D. H.; Johnson, D. C. *Chemistry of Materials* **1996**, *8*, 1853–1857.
- (4) Chiritescu, C.; Cahill, D. G.; Nguyen, N.; Johnson, D.; Bodapati, A.; Keblinski, P.; Zschack, P. *Science* **2007**, *315*, 351–353.
- (5) Karttunen, A. J.; Tynell, T.; Karppinen, M. *Nano Energy* **2016**, *22*, 338 – 348.
- (6) Lin, Q.; Smeller, M.; Heideman, C. L.; Zschack, P.; Koyano, M.; Anderson, M. D.; Kyky-

- neshi, R.; Keszler, D. A.; Anderson, I. M.; Johnson, D. C. *Chemistry of Materials* **2010**, *22*, 1002–1009.
- (7) Kohn, W.; Sham, L. J. *Phys. Rev.* **1965**, *140*, A1133.
- (8) Miara, L. J.; Richards, W. D.; Wang, Y. E.; Ceder, G. *Chemistry of Materials* **2015**, *27*, 4040–4047.
- (9) Rudin, S. P.; Johnson, D. C. *Phys. Rev. B* **2015**, *91*, 144203.
- (10) Warren, B. E. *Phys. Rev.* **1941**, *59*, 693–698.
- (11) Biscoe, J.; Warren, B. E. *Journal of Applied Physics* **1942**, *13*, 364–371.
- (12) Grosse, C.; Alemayehu, M. B.; Falmbigl, M.; Mogilatenko, A.; Chiatti, O.; Johnson, D. C.; Fischer, S. F. *Scientific Reports* **2016**, *6*, 33457 EP –.
- (13) Hite, O. K.; Johnson, D. private communication.
- (14) Kresse, G.; Furthmuller, J. *Phys. Rev. B* **1996**, *54*, 11169.
- (15) Kresse, G.; Joubert, D. *Phys. Rev. B* **1999**, *59*, 1758.
- (16) Perdew, J. P.; Burke, K.; Ernzerhof, M. *Phys. Rev. Lett.* **1996**, *77*, 3865.
- (17) Grimme, S. *Journal of Computational Chemistry* **2006**, *27*, 1787–1799.
- (18) Atkins, R.; Disch, S.; Jones, Z.; Haeusler, I.; Grosse, C.; Fischer, S. F.; Neumann, W.; Zschack, P.; Johnson, D. C. *Journal of Solid State Chemistry* **2013**, *202*, 128 – 133.
- (19) Kanematsu, K.; Ohoyama, T. *Journal of the Physical Society of Japan* **1965**, *20*, 236–242.
- (20) Henkelman, G.; Arnaldsson, A.; Jónsson, H. *Computational Materials Science* **2006**, *36*, 354 – 360.
- (21) Jain, A.; Ong, S. P.; Hautier, G.; Chen, W.; Richards, W. D.; Dacek, S.; Cholia, S.; Gunter, D.; Skinner, D.; Ceder, G.; Persson, K. a. *APL Materials* **2013**, *1*, 011002.

- (22) Cemic, L.; Neuhaus, A. *High Temperatures-High Pressures* **1972**, 4, 97–99.
- (23) Cook, W. R. *Journal of the American Ceramic Society* **1968**, 51, 518–520.
- (24) Elliott, N. *Journal of the American Chemical Society* **1937**, 59, 1958–1962.